



Article

Adsorption of As(V) at Humic Acid-Kaolinite-Bacteria Interfaces: Kinetics, Thermodynamics, and Mechanisms

Min Xiao ^{1,*} , Jingwen Guo ¹, Shan Zhao ¹ and Shifeng Li ^{2,*} 

¹ Key Lab of Eco-Restoration of Regional Contaminated Environment (Shenyang University), Ministry of Education, Shenyang 110044, China

² Liaoning Engineering Research Center for Treatment and Recycling of Industrially Discharged Heavy Metals, Shenyang University of Chemical Technology, Shenyang 110142, China

* Correspondence: xyz012263@163.com (M.X.); li.shi.feng@163.com (S.L.)

Abstract: The immobilization and transformation of arsenic at the mineral-organic interface in soil environments ultimately depend on the soil components and their interactions. Herein, the effect of humic acid (HA) and a typical bacterium (a Gram-positive *Bacillus subtilis*) coating on the adsorption of arsenate As(V) to kaolinite (Kao) mineral was investigated. The As(V) adsorption reaction kinetics, isotherms, thermodynamics, and mechanism on the clay mineral-organic composites of kaolinite-*Bacillus subtilis* (Kao-*B.s*) and humic acid-kaolinite-*Bacillus subtilis* (Kao-HA-*B.s*) were investigated. The As(V) adsorption on the composites was better fitted to pseudo-second-order kinetics and the Freundlich model. The adsorption capacity of As(V) followed the order of Kao-HA-*B.s* > Kao-*B.s* > *B.s* > Kao-HA > Kao. The positive ΔH (31.44, 5.87 kJ mol⁻¹) and ΔG (0.10–0.96 kJ mol⁻¹) values confirmed that the adsorption of As(V) by all composites was nonspontaneous and endothermic in character at room temperature. The FT-IR, XRD, and thermodynamic results revealed that the adsorption mechanism of As(V) on the kaolinite-organic interfaces could be attributed to the electrostatic forces between the terminal aluminum or silanol groups of kaolinite and As(V) and the complexation between HA, bacteria, and As(V), which formed an inner-sphere complex and surface complex, respectively. The experimental results showed that the adsorption of As(V) on the Kao-HA or Kao-bacteria system was accompanied by significant additive interactions, while the ternary Kao-HA-bacteria system had a significant inhibitory effect on As(V) binding at a higher HA content due to the shielding effect, with the promotion effect shown at a lower concentration for dispersion effect for HA on the kaolinite particles.

Keywords: kaolinite; arsenic; humic acid; bacteria; interface interactions



Citation: Xiao, M.; Guo, J.; Zhao, S.; Li, S. Adsorption of As(V) at Humic Acid-Kaolinite-Bacteria Interfaces: Kinetics, Thermodynamics, and Mechanisms. *Agronomy* **2023**, *13*, 611. <https://doi.org/10.3390/agronomy13020611>

Academic Editor: Maria Roulia

Received: 31 January 2023

Revised: 16 February 2023

Accepted: 17 February 2023

Published: 20 February 2023



Copyright: © 2023 by the authors. Licensee MDPI, Basel, Switzerland. This article is an open access article distributed under the terms and conditions of the Creative Commons Attribution (CC BY) license (<https://creativecommons.org/licenses/by/4.0/>).

1. Introduction

Arsenic is a metalloid pollutant of significant environmental concern due to its toxicity and widespread occurrence through volcanic eruption, the dissolution of ores and sediments, sewage disposal, mining, industry, and agriculture [1,2]. The immobilization and transformation of arsenic in complex systems in the soil environment mainly depend on its interactions with major soil components, such as minerals, soil organic matter, and micro-organisms [3,4]. About 50–90% of the dissolved organic carbon in soils and sediments is represented by humic acid (HA), which usually binds to minerals together with most micro-organisms [5] and forms mineral-organic aggregates through its functional groups such as carboxyl, phenol, amine, and hydroxyl [6–9]. The mechanisms for arsenic sorption on oxyhydroxides, clay minerals, humic acid, and micro-organism surfaces [7,10–14] have been widely conducted. The inner-sphere As(V) complexes on metal oxide surfaces were formed by surface complexation reactions through ligand exchange for the hydroxyl group; carboxylics, phenolics, and amines were considered to represent the most important group for the immobilization of As(V) on humic acid and bacteria, or a ternary system of humic

acid-inherent metal cation-arsenic was formed [1,7,14–16]. However, the surface characteristics and sorption properties of mineral-organic composites for arsenic varied greatly when compared to the crude component, especially in terms of the number of reactive sites, surface charge, and metal-binding affinity [17–19]. Kaolinite (Kao) is one of the most abundant clay minerals, for which the group mineral structure consists of tetrahedral (Si) and octahedral (Al) sheets stacked in 1:1 layers, and the chemical interactions between As(V) and kaolinite occur in the inner-surface hydroxyls of the octahedral through the formation of ligand structures [7,13,20,21].

The interactions of As(V) with clay mineral-organic complexes have not been systematically investigated, although numerous investigations have focused on bacterial attachment to pure or iron oxide-coated quartz [22–25] and kaolinite in the presence of HA [7,26,27] and binding to dissolved humic substances [1,28–30]. The effect of increasing As(V) adsorption on the modified kaolinite with HA was reported by Cornu et al. [27] in comparison with crude kaolinite, and HA significantly reduced the number of oxyanions adsorbed onto mineral surfaces [17,18]. Zhou et al. [12] and Fang et al. [31] discovered that the relative adsorption capacity and intensity of kaolinite for As(V) is higher with *Halobacillus* sp. Y35, and the components of the biofilm are not affected by minerals; the functional groups -OH, -NH, CH₂, -SH, -COO are responsible for metal ions binding [5]. A facilitating role and lower exothermic adhesion enthalpy were observed during HA coating on bacterial cell adhesion onto kaolinite combining electrostatic forces, chemical interactions, and the dispersion effect [32]. In ferrihydrite-organic-bacteria cosorption systems, the mineral was loosely associated with bacterial cells, whereas the ferrihydrite-HA composite was tighter, and As(V) reacted mainly with ferrihydrite. Consequently, understanding the adsorption behavior and mechanisms of As(V) on clay minerals in complex systems consisting of humic acid and/or bacteria would provide insights into predicting the fate and health risks of arsenic in the soil environment.

The aim of this study was to investigate the role, kinetics, and thermodynamic adsorption behavior of As(V) on the complexation of humic substances and/or bacteria with clay minerals in soil environments. kaolinite, humic acid, and Gram-positive *Bacillus subtilis* were selected as prototypes in this study, and the physicochemical characteristics, adsorption mechanism, and interaction on the binding of As(V) by the ternary composites of Mont/Kao-HA-bacteria were investigated by macroscopic sorption, together with XRD and FT-IR.

2. Materials and Methods

2.1. Materials

Kaolinite (Kao) was used as the clay mineral in this study and was purchased from Shanghai Yuanye Bio-technology Co., Ltd. (Shanghai, China). The kaolinite clays were ground to pass through an 80-mesh sieve. The mineral clay suspensions were prepared by dissolving, respectively, 50 g of each into 50 mL of Milli-Q water in a 1000 mL beaker and then treated with 15 mL of hydrogen peroxide (30%, solution) to remove the organic matter, and the excess of H₂O₂ was removed by evaporation [33]. The pH of the mineral solutions was adjusted to 9.0 for Kao by the addition of 0.1 mol·L⁻¹ NaOH and was dispersed by ultrasonic for 30 min. The dispersions were diluted to 1000 mL with Milli-Q water, and the <2 μm colloidal fractions were isolated by sedimentation using the pipette method [34]. The separated colloid dispersions were then flocculated with 0.5 mol·L⁻¹ CaCl₂ solutions, and then the particles were washed with Milli-Q water until negative Cl⁻, determined by AgNO₃ resolution. Finally, the minerals obtained were crushed to pass through a 100-mesh sieve after drying at 60 °C and stored for subsequent utilization.

Humic acid (HA) was supplied by Shanghai Yuanye Bio-technology Co., Ltd. (Shanghai, China), and was extracted from commercial peat by dissolving with 1.0 mol·L⁻¹ NaOH, filtered at 0.45 μm three times, and then it was precipitated with 1.0 mol·L⁻¹ HCl at a pH below 1.5, subsequently recovered by centrifugation and rinsed with Milli-Q water, finally rinsed with Milli-Q water to remove excess salt. The stock HA solution was prepared by dis-

solving with $1.0 \text{ mol}\cdot\text{L}^{-1}$ NaOH at pH 8.0, filtered at $0.45 \mu\text{m}$ three times, and stored at $4 \text{ }^\circ\text{C}$. The HA working solutions were prepared by dilution with $0.01 \text{ mol}\cdot\text{L}^{-1}$ NaNO_3 electrolyte and then dispersed in an ultrasonic bath for 10 min prior to use. The dissolved organic carbon concentrations of the HA solution were determined with an ELEMENTAR-TOC carbon analyzer (LiquiTOC/TNb, Hanau, German).

The Gram-positive *Bacillus subtilis* strain (CCTCC AB 90008, *B. subtilis*) was supplied by the China Center for Type Culture Collection (Wuhan, Hubei, China). The *B. subtilis* strain was initially inoculated in Luria-Bertani (LB) nutrient medium ($10.0 \text{ g}\cdot\text{L}^{-1}$ tryptone, $5.0 \text{ g}\cdot\text{L}^{-1}$ yeast extract, $5.0 \text{ g}\cdot\text{L}^{-1}$ NaCl) for 24–36 h at $37 \text{ }^\circ\text{C}$; then the bacterial cells were cultivated to the late-exponential growth for 7–8 h at $28 \text{ }^\circ\text{C}$, followed by expanding culture at a ratio of 1:100 for another 18 h. The fresh biomass was harvested by centrifugation at 5000 rpm for 12 min to harvest the cells, followed by three washing procedures with $0.1 \text{ mol}\cdot\text{L}^{-1}$ NaNO_3 electrolyte. The cell pellets were resuspended in the electrolyte ($0.1 \text{ mol}\cdot\text{L}^{-1}$ NaNO_3) to form a parent solution and stored at $4 \text{ }^\circ\text{C}$. 1 mL of the suspension was taken and dried to constant weight at $60 \text{ }^\circ\text{C}$ to determine the bacterial concentration. The fresh *B. subtilis* biomass was used for the later adsorption experiments within 12 h to ensure bacterial activity and to minimize the production of bacterial secretions in this study. The bacteria obtained were resuspended with $0.01 \text{ mol}\cdot\text{L}^{-1}$ NaNO_3 solution.

NaCl, NaNO_3 , HNO_3 , and NaOH were of analytical reagent grade and were purchased from Sinopharm Chemical Reagent Shenyang Co., Ltd. (Shenyang, Liaoning, China).

Arsenate stock solutions ($1000 \text{ mg}\cdot\text{L}^{-1}$) were prepared by dissolving $\text{Na}_2\text{HAsO}_4\cdot 7\text{H}_2\text{O}$ in ultrapure water, and the required dilutions were obtained daily prior to use. The initial pH of the solutions was adjusted to 5.0 with $0.1 \text{ mol}\cdot\text{L}^{-1}$ NaOH and HNO_3 , and the constant ionic strength was maintained with a $0.01 \text{ mol}\cdot\text{L}^{-1}$ NaNO_3 electrolyte solution. Hydrochloric acid, sodium hydroxide, and sodium borohydride were purchased from Adamas.

2.2. Preparation of the Composites

The mineral was suspended in $0.01 \text{ mol}\cdot\text{L}^{-1}$ NaNO_3 electrolyte for subsequent utilization and was dispersed in an ultrasonic bath for 10 min prior to use.

The binary Kao-*B.subtilis* mixture was formed at initial mass mineral to bacteria ratios of 1, 10, and 100 (dry weight basis). The Kao-*B.subtilis* suspensions were immediately shaken and adjusted to the chosen pH values by dropwise addition of $0.1 \text{ mol}\cdot\text{L}^{-1}$ HNO_3 and NaOH solutions and then allowed to equilibrate for 4 h at $28 \text{ }^\circ\text{C}$ in a shaker to achieve kaolinite-bacteria adhesion equilibrium. The mixture was then used for the adsorption experiments without any washing procedure.

The humic acid and kaolinite complex (Kao-HA) was obtained by mixing 2.0 g Kao and 200 mL HA working suspension ($100, 500, 800, 1200, 1500 \text{ mg}\cdot\text{L}^{-1}$) in a 500 mL conical flask, NaOH, and HNO_3 solutions ($1.0 \text{ mol}\cdot\text{L}^{-1}$) were used to adjust the pH of the suspension to 5.0, and the ionic strength was maintained with a background electrolyte of $0.1 \text{ mol}\cdot\text{L}^{-1}$ NaNO_3 , then the resulting Kao-HA complex suspension was shaken at $28 \text{ }^\circ\text{C}$ for 24 h. Subsequently, the suspension was centrifuged at $8000\times g$ for 12 min to harvest the samples and rinsed three times with $0.01 \text{ mol}\cdot\text{L}^{-1}$ NaNO_3 solution until neither the supernatant became colorless nor HA particulates accumulating on the top of kaolinite fractions after centrifugation were visualized. Finally, the residue was air-dried at $45 \text{ }^\circ\text{C}$, ground to pass through a 200-mesh sieve, and stored for future use. The excess HA remaining in the supernatant (including loss during the washings) was measured in a UV-vis spectrophotometer at 314 nm, and the amount of HA bound to kaolinite was then calculated.

The Kao-HA composite prepared above was suspended in $0.01 \text{ mol}\cdot\text{L}^{-1}$ NaNO_3 , and the Kao-HA-*B.subtilis* ternary composites were formed by adding *Pseudomonas putida* parent suspensions ($10 \text{ g}\cdot\text{L}^{-1}$) dropwise to the Kao-HA suspension, adjusting the pH to 5.0. The ternary composite was shaken for 24 h at $25 \text{ }^\circ\text{C}$, separated by centrifugation ($8000\times g$ for 12 min), and washed three times with electrolyte. The supernatants were subjected to

UV-spectrophotometry, which showed that no free HA was released from the composites (<1%). The solid phase was suspended in 0.01 mol·L⁻¹ NaNO₃ electrolyte. The final mass ratios of each fraction (dry-weight basis) in the ternary composites were 50:1:50 and 100:5:1 for Mont: HA: bacteria (denoted as Kao: HA: *B.subtilis* = 50:1:50, 100:5:1). The Kao-HA-bacteria composites were used for subsequent experiments.

2.3. Characterization

The crystal structure of Kao and Kao-organic aggregates before and after absorption of As(V) was characterized by XRD (Rigaku: Ultima IV, Tokyo, Japan) diffractometer at Cu K α radiation and a fixed power source (40 kV and 40 mA) with diffraction angle (2 θ) ranging from 5° to 70°. The field emission scanning electron microscope (FE-SEM, HITACHI S-4800, Tokyo, Japan) was used to observe the surface morphology of Kao-organic aggregate samples. FT-IR spectra were determined by the accumulation of 256 scans with a resolution of 2 cm⁻¹ within the range of 450–4000 cm⁻¹ (Thermo Fisher Nicolet 670, Waltham, MA, USA). The As(V) concentration was determined by hydride generation atomic fluorescence absorption spectrophotometric analysis (Jinsuokun SK-2003AZ, Beijing, China) [12]. Experimental samples before and after As(V) adsorption were separated by centrifugation (8000 × g for 12 min), freeze-dried (Labconco FreeZone, Kansas City, MO, USA), and ground prior to further analysis. Cell morphology of Kao-*B.subtilis* and Kao-HA-*B.subtilis* composites before and after As(V) adsorption (within 12 h after the end of each adsorption experiment), was observed using an Olympus CX23 confocal microscope (Olympus Corporation, Tokyo, Japan) and photographed at ×40 magnification.

2.4. Adsorption Study

Adsorption experiments were conducted in batch mode with the minerals and their composites (bacteria and HA) in a 50 mL plastic tube. Synthetic As(V) solution (2.5 mg·L⁻¹) was added to a conical flask with an adsorbent dosage of 2.5 g·L⁻¹. Samples were taken at certain intervals and filtered through a 0.45 μ m nitrocellulose membrane filter to measure the residual As(V) concentration.

The adsorption isotherms experiments were performed at an initial pH of 5.0 and 25–45 °C, conducted with 20 mL As(V) solution (0.5 to 40 mg·L⁻¹) with electrolyte solutions in 50 mL polyethylene centrifuge tubes, and the dosage of the composite sorbent (Kao, Kao-HA, Kao-*B.subtilis*, and Kao-HA-*B.subtilis*) was 1.0 g·L⁻¹, the suspensions were elliptically shaken for 24 h until the adsorption equilibrium was reached. The samples were then separated by centrifugation (8000 × g for 12 min) for analysis, and the residual concentration of As(V) in the clear supernatant solution was determined accordingly. The adsorption degree of As(V) was determined as follows:

$$q_e = \frac{(C_0 - C_e) \cdot V}{m} \quad (1)$$

where q_e represents the adsorption capacity of Cu²⁺ or Cd²⁺ at equilibrium time min (mg·g⁻¹); C_0 and C_e are the initial and final concentrations of the heavy metal concentrations (mg·L⁻¹). V is the volume of the solution, and m is the weight of the sorbent (g).

The Freundlich adsorption processes were as follows:

$$q_e = k_f C_e^n \quad (2)$$

where q_e is the maximum adsorption capacity of As(V), whereas k_f , n represent the adsorption constants of Freundlich models.

The adsorption kinetics experiments were conducted as follows: Kao, Kao-HA, Kao-*B.subtilis*, or Kao-HA-*B.subtilis* composites were added to 0.01 mol·L⁻¹ NaNO₃ solutions with initial As(V) concentrations of 2.5 mg·L⁻¹. The pH of the reaction systems was kept at 5.0 throughout the experiments. Samples of 5 mL were then withdrawn at different time intervals (0, 5, 10, 15, 20, 30, 45, 60, 90, 120, 180, 300, and 480 min). Residual As(V)

concentrations in water were measured after filtering the samples through 0.45 µm nylon filter membranes. The concentration of As(V) in the filtrate was then analyzed using a hydride generation-atomic fluorescence spectrophotometer. A pseudo-first-order and a pseudo-second-order model were applied to investigate the adsorption kinetics [35]:

$$\lg(q_e - q_t) = \lg q_e - \frac{K_1}{2.303} t \quad (3)$$

$$\frac{t}{q_e} = \frac{1}{k_2 q_e^2} + \frac{t}{q_e} \quad (4)$$

where q_e and q_t represent the adsorption capacity of As(V) at the pseudo-equilibrium condition and at time t , respectively (mg/g); k_1 and k_2 are the adsorption rate constants.

Meanwhile, three sets of batch adsorption experiments were carried out as a function of solution pH, ionic strength of the solution, composite types, and ratio on As(V) adsorption, respectively. The effect of pH on As(V) sorption was investigated from 3–10 using 0.1 mol·L⁻¹ HNO₃ or 0.1 mol·L⁻¹ NaOH, and the final pH of the suspension after the equilibration time was mentioned. The relationship between the ionic strength and As(V) adsorption was carried out with the background electrolyte 0.01, 0.1, and 1 mol·L⁻¹ NaNO₃. HA concentration (from 0.3% to 6.7%) and the binary or ternary composite types were also performed to study the interaction of As(V) with mineral-organo composites. Following the adsorption equilibration, the suspension was centrifuged at 8000 × g for 12 min. The supernatant was filtered through 0.45 µm nylon filter membranes and collected for As(V) analysis.

All experiments were performed in triplicate, and the average values are reported here. A portion of the samples was dried for XRD and FTIR analysis.

3. Results and Discussion

3.1. The Effect of the Initial As(V) Solution pH

The surface charge of the adsorbent particles, the anionic forms of As(V), and the degree of ionization were dependent on the solution pH [36]. As shown in Figure 1, As(V) adsorption on Kao-organic composites gradually decreased with pH from 3.0 to 7.0, and a drastic drop in As(V) uptake at pH > 7 is observed. The sorption of As(V) on Kao-HA-*B.subtilis* was higher than that of Kao-*B.subtilis*, and lower at a higher HA content. The functional groups -OH, -NH, CH₂, -SH, and -COO of *Bacillus subtilis* (CCTCC AB 90008) and HA played a key role in the As(V) adsorption, although negatively charged bacterial cells/HA could enhance the electrostatic repulsion between As(V) and Kao, *Bacillus subtilis* (CCTCC AB 90008) seemed stronger than that of HA in enhancing As(V) sorption, which agrees with previous studies [3,37–39]. Attachment on the ternary Kao-HA-*B.subtilis* composite was higher than that of the binary composite, indicating the advantage of the dispersion of kaolinite particles in the presence of HA under the multifactorial function of electrostatic forces, chemical interactions, steric hindrance, and mineral aggregation. This outcome was contrary to the classical Overbeek (DLVO) theory and the reduction of reactive surface sites through complexation reactions, and the bridging mechanism was proposed by Walker et al. for Cu²⁺ and Pb²⁺ adhesion on *Escherichia coli* cell envelopes-kaolinite composite [40–42]. However, a similar decreasing aggregation phenomenon was reported by Z. Hong et al. [32] for the effect of HA on the adhesion of *Bacillus subtilis* to kaolinite, providing more surface area for cell adhesion. The ionization of the weak arsenic acid depended on the corresponding pK_a values (pK_{a1} = 3.60, pK_{a2} = 7.25, and pK_{a3} = 12.25), the H₃AsO₄ molecular form present at a pH of < 2.3, and the deprotonated AsO₄³⁻ form (pH > 11); the dissociated H₂AsO₄⁻ and HAsO₄²⁻ were predominant at a pH from 2.3 to 5 and 7 to 10, respectively. In the range of pH 3.0–6.0, the speciation of As(V) showed H₂AsO₄⁻ dominance, whereas HAsO₄²⁻ was predominant at pH 8 and 10. The direct proton transfer due to the amphoteric hydroxyl groups (-OH) determined the surface charge of the minerals. Since the zero-point charge (pH_{ZPC}) for kaolinite is pH 2.3, at which the net charge on the surface is neutral, H₂AsO₄⁻ could easily attach to the

surface of kaolinite-organo composites in a low acidic medium, while the surface became increasingly negative: superior to the pH_{pzc} , more As(V) remained in the solution due to strong electrostatic repulsion with As(V) species (HAsO_4^{2-} and AsO_4^{3-}). Furthermore, the adsorption of As(V) was observed to increase around pH 5, suggesting that the formation of an Al-organo-As composite was due to surface complexation reactions interfering with the interaction of As(V) with kaolinite; As(V) preferentially bound to the anions of $\text{Al}_2\text{OH}^{2+}$ and SiO^- rather than to the OH^- ions.

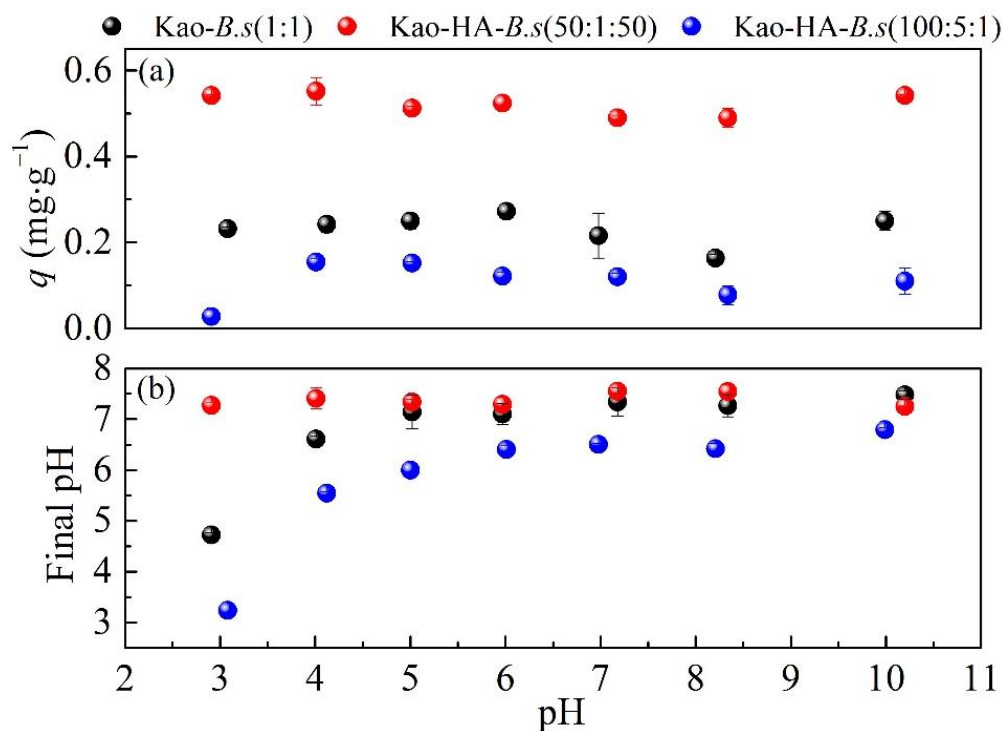


Figure 1. Effect of pH on As(V) adsorption onto kaolinite composites: (a) pH & q ; (b) $\text{pH}_{\text{initial}}$ & pH_{final} (C_0 : $2.5 \text{ mg}\cdot\text{L}^{-1}$; adsorbent dosage: $2.5 \text{ mg}\cdot\text{L}^{-1}$; T : 25°C ; Ionic strength: $0.01 \text{ mol}\cdot\text{L}^{-1}$; t : 24 h).

Based on the modeling of As(V) adsorption on kaolinite, it is shown that bidentate ligands are favored at a lower pH, while monodentate ligands are favored at high pH values [12,21]. Furthermore, the adsorption rate is mainly controlled by the surface binding energy at the solid–liquid interface, which tends to have a higher adsorption rate. The binding power of Kao-HA-*B.subtilis* (plus the As(V) system) was greater than that of the Kao-*B.subtilis* system for increasing the absolute values of the zeta potential.

In addition, after adsorption, the pH_{final} values tended to be neutral because the hydroxylated surface of the composites was modified by amphoteric dissociation. The adsorption capacity of the Kao-*B.subtilis* system was obviously lower than that of the Kao-HA-*B.subtilis* system within all experimental pH ranges.

Figure 1b revealed that there was a significant capacity for the ternary humic acid-kaolinite-bacteria composite (50:1:50) to buffer highly acidic and alkaline systems, which was in agreement with the data from other published As(V) adsorptions onto minerals [37,38].

3.2. Effect of Ionic Strength

The influence of ionic strength on As(V) adsorption onto the coating of *B. subtilis* and humic acid with kaolinite was shown in Figure 2.

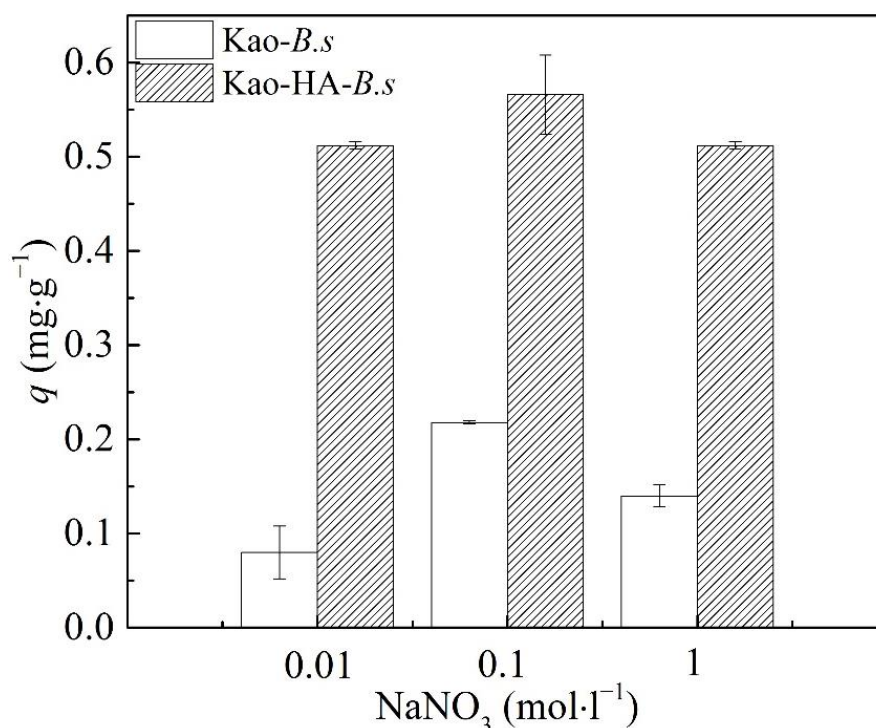


Figure 2. Effect of ionic strength on As(V) adsorption on Kao-*B.s* and Kao-HA-*B.s* (50:1:50) complexes (C_0 : 2.5 mg·L⁻¹; adsorbent dosage: 2.5 mg·L⁻¹; T: 25 °C; pH: 5; t: 24 h).

The amount of As(V) sorption with the Kao-*B.subtilis* and Kao-HA-*B.subtilis* (50:1:50) composites first increased and then decreased with ionic strength. The As(V) adsorption capacity increased from 0.08 to 0.22 mg·g⁻¹ for the Kao-*B.subtilis* system and from 0.51 to 0.57 mg·g⁻¹ for the Kao-HA-*B.subtilis* ternary one with increasing ionic strength (from 0.01 to 0.1 mol·L⁻¹). The surface modification of kaolinite by humic acid could enhance the adhesion of *B. subtilis*, indicating that the dispersion effect of HA on kaolinite dominated the adsorption process. These trends are consistent with the previously reported results [32,43]. Clay minerals could form an internal ligand structure with arsenic due to the aluminum oxide octahedron in their system, and the bonds at the edges of the outer surface were broken, making the edges have oxide-like characteristics [44]. As the ionic strength increased, some of the H⁺ on the surface of the oxide could be replaced by more and more Na⁺ and released into the solution. This promoted the adsorption of As(V).

However, increasing the ionic strength would increase the net negative charge on the HA molecules and decrease the point of zero charges [45], resulting in a decrease in arsenic sorption.

3.3. Effect of Composite Type and Proportion

Humic acid is an essential component of soil organic matter. Proportions of the mineral-organic composites were used to investigate the effect of HA and bacteria on As(V) adsorption on the kaolinite layer. As shown in Figure 3a, the maximum As(V) adsorption capacities followed the order of Kao-HA-*B.s* (50:1:50) > Kao-*B.s* > *B.s* > Kao-HA-*B.s* (100:5:1) > Kao-HA > Kao, indicating the enhancing effect of HA and *Bacillus subtilis* on As(V) adsorption. The adsorption performance in the ternary system (Kao-HA-*B.s*) was inhibited at higher HA content compared to the mineral-bacteria binary system, indicating that a strong adsorption site masking effect [24,32] developed in the Kao-HA-*B.subtilis* ternary system at higher HA concentrations, and the interaction of As(V) with bacterial functional groups was blocked by humic acid through site-specific reactions.

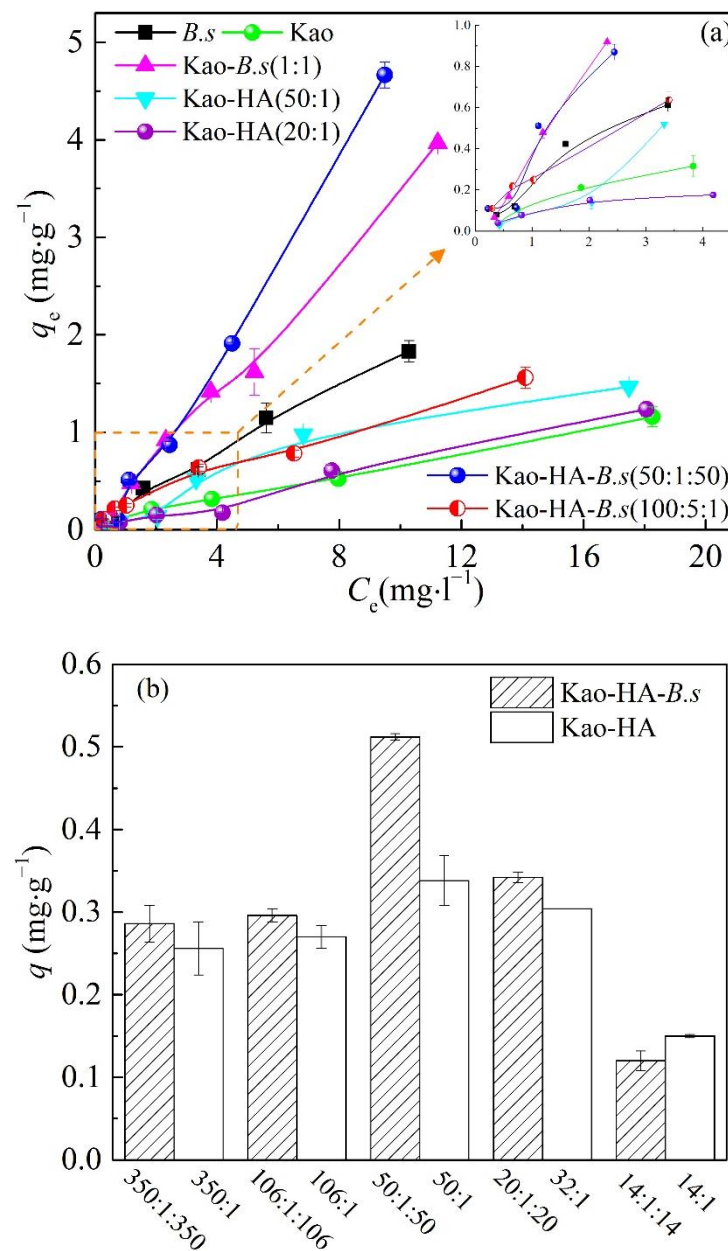


Figure 3. Effect of composite types on As(V) adsorption on Kao-*B.s* and Kao-HA-*B.s* ((a) C_0 : 0.5–21.15 mg·L⁻¹; (b) C_0 : 2.5 mg·L⁻¹; adsorbent dosage: 2.5 mg·L⁻¹; T: 25 °C; ionic strength: 0.01 mol·L⁻¹; t: 24 h).

The promotion of As(V) by HA was observed at lower doses of HA (from 0.3% to 2.0%), which can be seen in Figure 3a,b. The enhancement of *Bacillus subtilis* adhesion to kaolinite by HA coatings had been found due to the decrease in the aggregation of kaolinite [40], for which the physicochemical interfacial process, which was enhanced with As(V) species. However, the adsorption experiments showed the inhibition of As(V) adsorbed on kaolinite at a higher HA dosage (from 4.8% to 6.7%). The adsorption property strongly supported competition between HA and As(V) for the binding sites on the mineral surfaces. The crystal edges or broken bonds of the mineral surface chemical structure determined the adsorption capacity of the clay minerals [46]. The adsorption of humic acid on kaolinite was shown via adsorption modeling to be a combination of inner-sphere complex monodentate ligands and outer-sphere H-bonds. In contrast, the inner-sphere bidentate ligands dominated during As(V) adhesion, with a smaller percentage forming monodentate ligands [47]; thus, the HA had a stronger affinity for Kao than that of As(V).

3.4. Adsorption Kinetics

The As(V) adsorption kinetic curves of As(V) on Kao-*B.subtilis* and Kao-HA-*B.subtilis* (50:1:50) are presented in Figure 4; the adsorption equilibrium time in the ternary system was approximately 300 min regarding the Kao-*B.subtilis* composite, whereas it took about 1000 min for the Kao-HA-*B.subtilis* system. The pseudo-first-order and pseudo-second-order models were applied to research the adsorption kinetics [35], and the calculated kinetic parameters are summarized in Table 1 via the plot in Figure 5a,b. As shown in Figure 5, the pseudo-second-order equation provided higher values of correlation coefficients than 0.999 for As(V) when compared with the other one, and the modeled sorption capacity was in accordance with the obtained experimental data, indicating that chemisorption controlled the adsorption process for As(V), and the mineral-organic composites were controlled by the sharing or exchanging of electrons between the As(V) and composites [13]. As presented in Table 1, the kinetic data showed a faster adsorption rate for the Kao-HA-*B.subtilis* system than the Kao-*B.subtilis* system regarding the adsorption capacity towards As(V), indicating that the adsorption site and porosity of the Kao-HA-*B.subtilis* ternary system increased at a lower HA content.

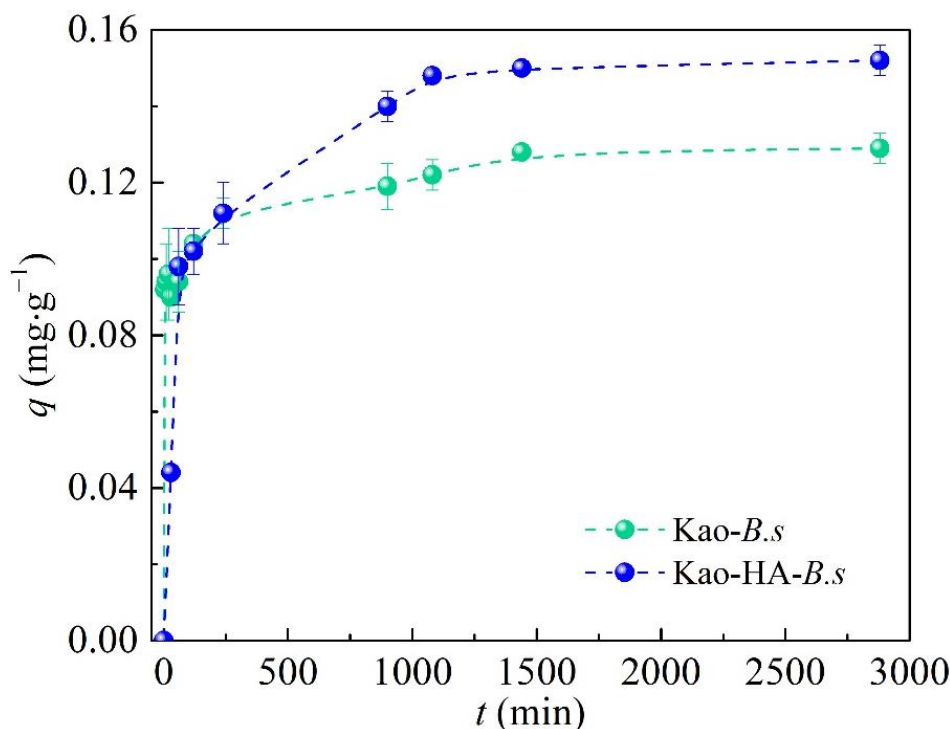


Figure 4. The adsorption kinetics of As(V) on Kao-*B.s* and Kao-HA-*B.s* (50:1:50) (C_0 : 1.0 mg·L⁻¹; adsorbent dosage: 2.5 mg·L⁻¹; T: 25 °C; ionic strength: 0.01 mol·L⁻¹; pH: 5).

Table 1. Adsorption kinetics parameters for As(V) on Kao-*B.s* and Kao-HA-*B.s* (50:1:50).

Model	Parameters	Kao- <i>B.s</i>	Kao-HA- <i>B.s</i>
Pseudo-first-order	k_1 (min ⁻¹)	0.00205	0.00253
	q_e (mg·g ⁻¹)	0.0372	0.0794
	R^2	0.89235	0.95943
Pseudo-second-order	k_2 (mg·g ⁻¹ min ⁻¹)	0.329	0.0934
	q_e (mg·g ⁻¹)	0.129	0.156
	R^2	0.99915	0.99944

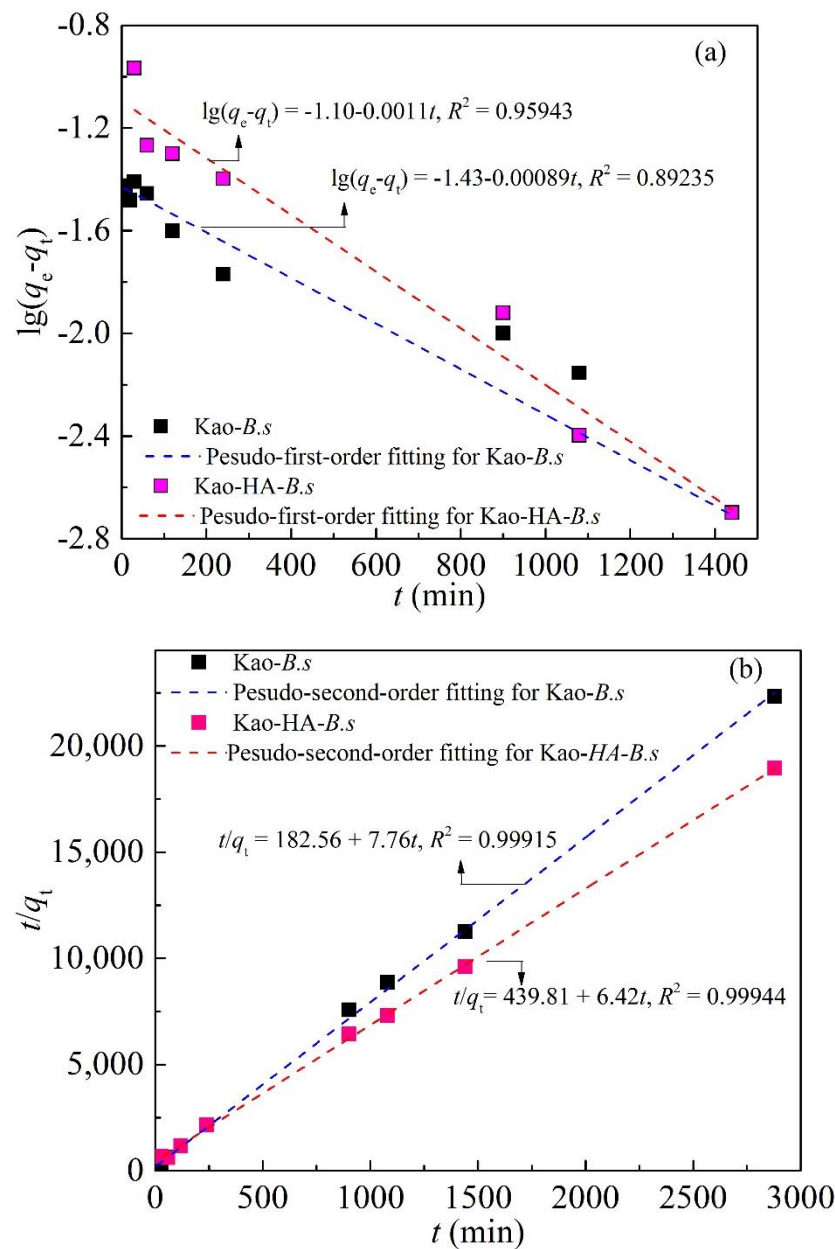


Figure 5. The adsorption kinetics of As(V) on Kao-B.s (a) and Kao-HA-B.s (50:1:50) (b) (C_0 : $1.0 \text{ mg}\cdot\text{L}^{-1}$; adsorbent dosage: $2.5 \text{ mg}\cdot\text{L}^{-1}$; T: $25 \text{ }^\circ\text{C}$; ionic strength: $0.01 \text{ mol}\cdot\text{L}^{-1}$; pH: 5).

3.5. Adsorption Isotherms

Figure 6a,b shows the adsorption isotherms of As(V) on Kao-B.*subtilis* and the Kao-HA-B.*subtilis* (50:1:50) systems at different temperatures ($26\text{--}45 \text{ }^\circ\text{C}$). The obtained adsorption isotherm data can be described by the Freundlich equation (Figure 6c), and the relative parameters are summarized in Table 2. The high correlation coefficients showed that the As(V) adsorption on Kao-B.*subtilis* and Kao-HA-B.*subtilis* systems fitted the Freundlich isotherm, indicating that the kaolinite-organic complexes had multilayer adsorption sites for As(V). The value of q for As(V) adsorption was positively correlated with temperature, which was consistent with those reported in the literature [48]. Furthermore, As(V) was prone to adsorb onto the surfaces of the Kao-HA-B.*subtilis* complexes at room temperature owing to the lower $1/n$.

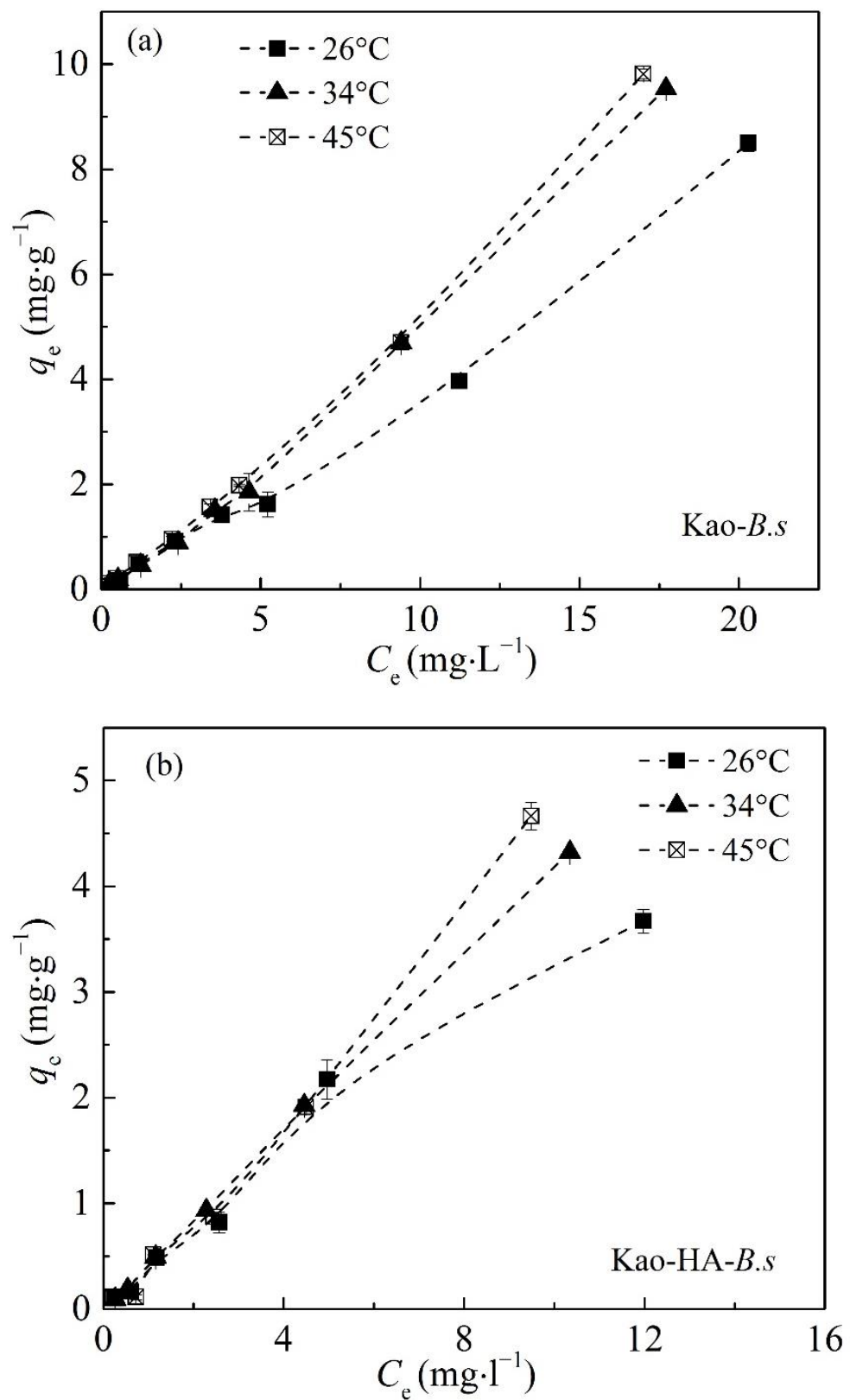


Figure 6. Cont.

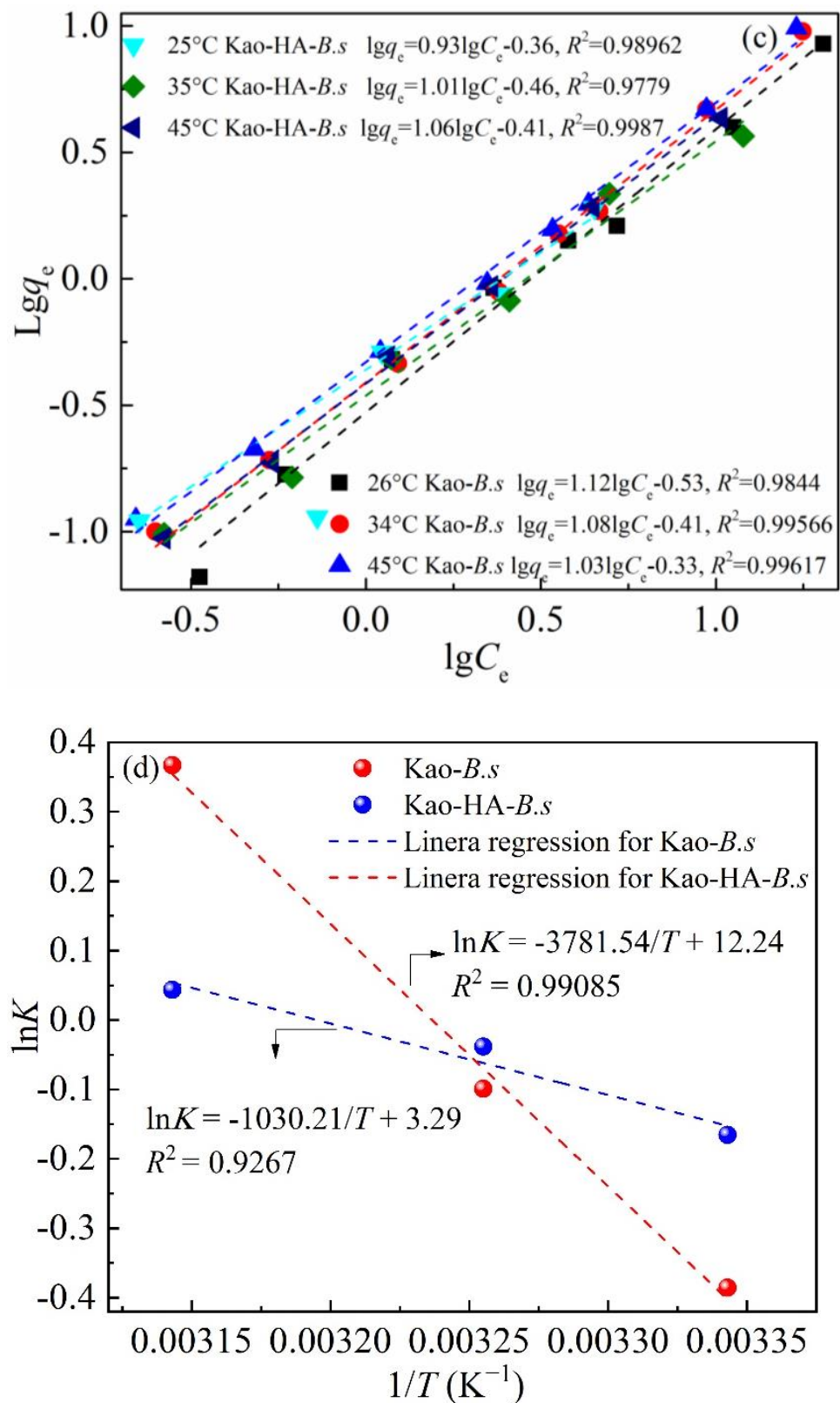


Figure 6. As(V) adsorption isotherms on Kao-B.s (a) and Kao-HA-B.s (50:1:50) (b), Freundlich model fitting (c) and plot of $\ln k$ versus $1/T$ (d) (Adsorbent dosage: 2.5 mg·g⁻¹; pH: 5; ionic strength: 0.01 mol·L⁻¹; t: 48 h).

Table 2. Parameters for As(V) adsorption on Kao-B.s and Kao-HA-B.s systems by Freundlich isotherm models.

Temperature (°C)	Kao-B.s			Kao-HA-B.s (50:1:50)		
	Freundlich Parameters			Freundlich Parameters		
	k_f (mg·g ⁻¹)	1/n	R ²	k_f (mg·g ⁻¹)	1/n	R ²
26	0.295	1.12	0.9844	0.437	0.93	0.98962
34	0.389	1.08	0.99566	0.347	1.01	0.9779
45	0.468	1.03	0.99617	0.389	1.06	0.9987

The As(V) adsorption thermodynamic parameters, equilibrium constant K , and enthalpy (ΔH°) were obtained as the values that gave the best fit for this expression (to the cumulative heat release curves) (Figure 6b). The Gibbs free energy (ΔG°) and entropy (ΔS°) for As(V) adsorption can be calculated according to Equations (5)–(7), and the results of the thermodynamic parameters are given in Table 3.

$$\Delta G^\circ = -RT \ln K \quad (5)$$

$$K = \frac{C_a}{C_s} \quad (6)$$

$$\ln K = \frac{\Delta S^\circ}{R} - \frac{\Delta H^\circ}{RT} \quad (7)$$

where T was the solution temperature (K), R was the gas constant (J·mol⁻¹·K⁻¹), and C_a and C_s were the equilibrium concentrations of As(V) on the adsorbent and in the solution, respectively.

Table 3. Thermodynamic parameters of As(V) adsorption on Kao-B.s and Kao-HA-B.s (50:1:50).

T(K)	As R%		ΔG (kJ·mol ⁻¹)		ΔH (kJ·mol ⁻¹)		ΔS (J·mol ⁻¹ ·K ⁻¹)	
	Kao-B.s	Kao-HA-B.s	Kao-B.s	Kao-HA-B.s	Kao-B.s	Kao-HA-B.s	Kao-B.s	Kao-HA-B.s
299.15	45.57	45.95	0.96	0.41				
307.15	51.01	48.98	0.25	0.10	31.44	8.57	101.76	27.35
318.15	59.02	51.07	-0.97	-0.12				

From Table 3, it can be seen that ΔG and ΔH are positive at lower temperatures, indicating that the adsorption process is nonspontaneous and endothermic. In contrast, the negative values of ΔG at 45 °C indicate the spontaneous and exothermic adsorption reaction of As(V) on the kaolinite-organic complexes. As shown in Table 3, the adsorption of As(V) by all composites was a spontaneous entropy-increase reaction, indicating that the inner-sphere complexes were formed during the adsorption process [37,49–51].

3.6. Characterization of Kao-Organic Aggregates

As mentioned above, the binding strength for As(V) bound the ternary system more strongly than the binary system. The properties of the clay minerals and their composites before and after the adsorption were investigated by SEM, optical microscopy, XRD, and FTIR characterization.

3.6.1. SEM and Optical Microscopy Analyses

The morphology images of kaolinite, humic acid, *B.subtilis*, and the Kao-organic aggregates before and after As(V) adsorption are shown in Figures 7 and 8.

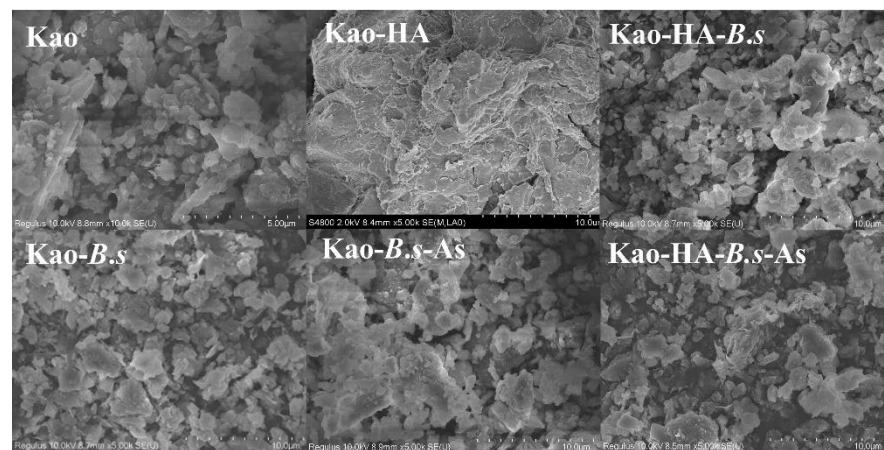


Figure 7. SEM images of composites before and after As(V) adsorption.

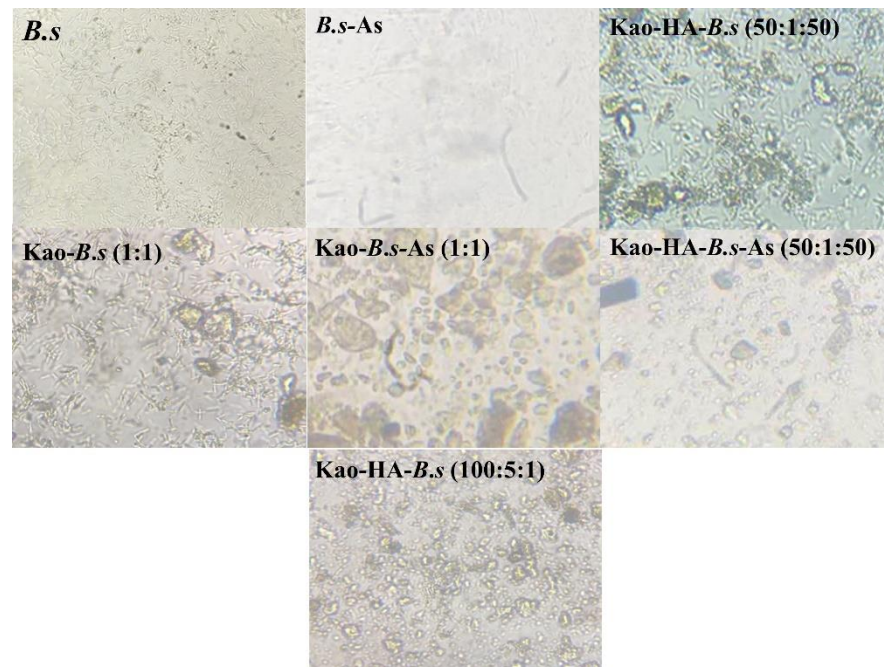


Figure 8. Optical microscopy of composites before and after As(V) adsorption.

Kaolinite showed a layered hexagonal shape with a size mostly smaller than 2 μm . The kaolinite grains tend to clump together but do not produce a compact mineral film with plenty of naked cell surface. The humic acid was adsorbed on the kaolinite particle surfaces and produced compact aggregates. This close association for our Kao-HA adsorbed composite was similar to those reported in the Kao-organo composites formed via a coprecipitation procedure [24,40]. The bacterial cells tend to be “glued” together, possibly through the agglutination of extracellular polymers. The association between the kaolinite and the cells was not tight enough to produce a compact mineral film. An aggregated phenomenon in a pure mineral system was found, but the kaolinite particles were more dispersed in the bacteria mixtures; the surface adsorption sites for metals in the kaolinite-bacteria composite were sufficient in each end-member component. The enhancement of *Bacillus subtilis* adhesion to kaolinite by HA coatings was found due to a decrease in the aggregation of kaolinite, for which the physicochemical interfacial process was enhanced by As(V) species.

3.6.2. XRD Analysis

The XRD patterns of kaolinite, HA, *Kao-B.subtilis*, and the *Kao-HA-B.subtilis* composites before and after the reaction of As(V) are shown in Figure 9.

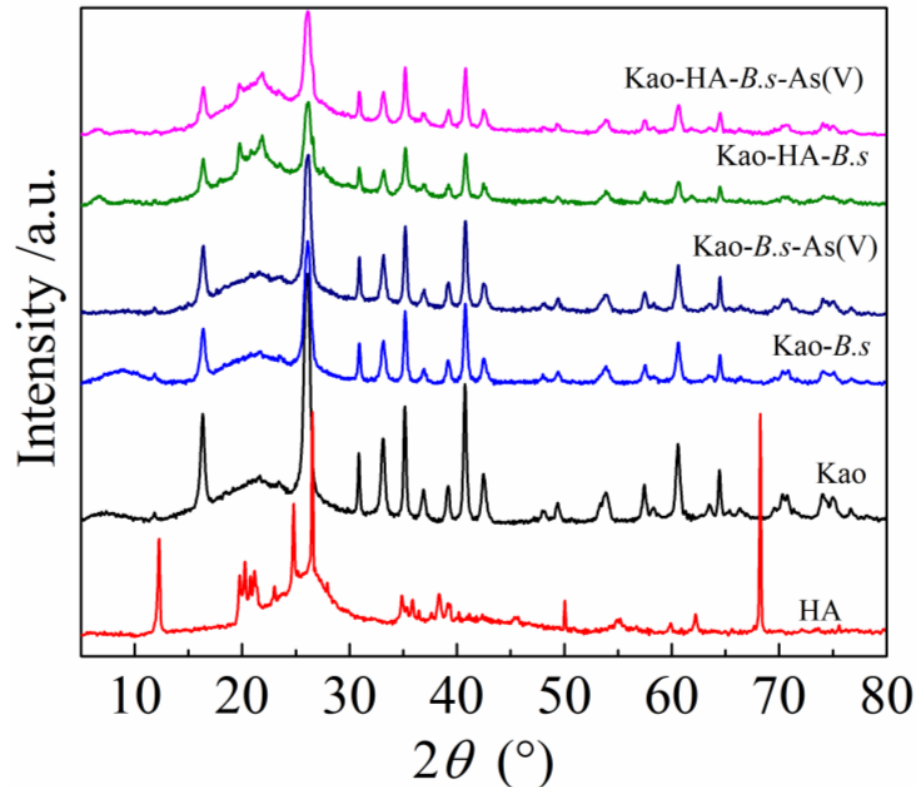


Figure 9. XRD pattern of composites before and after As(V) adsorption.

The peaks at 16.37° and 25.98° are assignable to the typical characteristic diffraction pattern of kaolinite, corresponding to (001) and (002) of kaolinite (JCPDS No. 01-080-0886), respectively. There was no significant change in the basal spacing of the kaolinite after the adsorption of HA or bacteria, indicating that they were not intercalated into the interlayer of the kaolinite due to the large molecule structure, which was also reported by Wu and Chassapis et al. [52,53]. In contrast, interlayer spacing increased from 0.5411 nm to 0.55 nm for the *Kao-B.subtilis* *Kao-HA-B.subtilis* complexes upon the reaction with As(V), revealing that the inner-sphere complex for the *Kao-B.subtilis* and *Kao-HA-B.subtilis* composites.

The increase in this interlayer spacing in the *Kao-B.subtilis* system suggested that As(V) could penetrate the bacteria in the outer layer banded with carboxyl groups and form various inner-sphere complexes with kaolinite due to the variable charges in the latter gibbsite basal planes [54,55] or the arsenic ions that were initially adsorbed on bacterial and/or humic acid surfaces (at lower HA content), which were bound to the lower potential of humic acid [56]. As the reaction proceeded, they would gradually transfer to the high potential energy mineral functional groups through chemical bonds or co-ordinate covalent bonds, thus forming an internal layer complex.

3.6.3. FTIR Analysis

The FT-IR spectra of the binary *Kao-HA* and ternary *Kao-HA-bacteria* complexes before and after reaction with As(V) are shown in Figure 10.

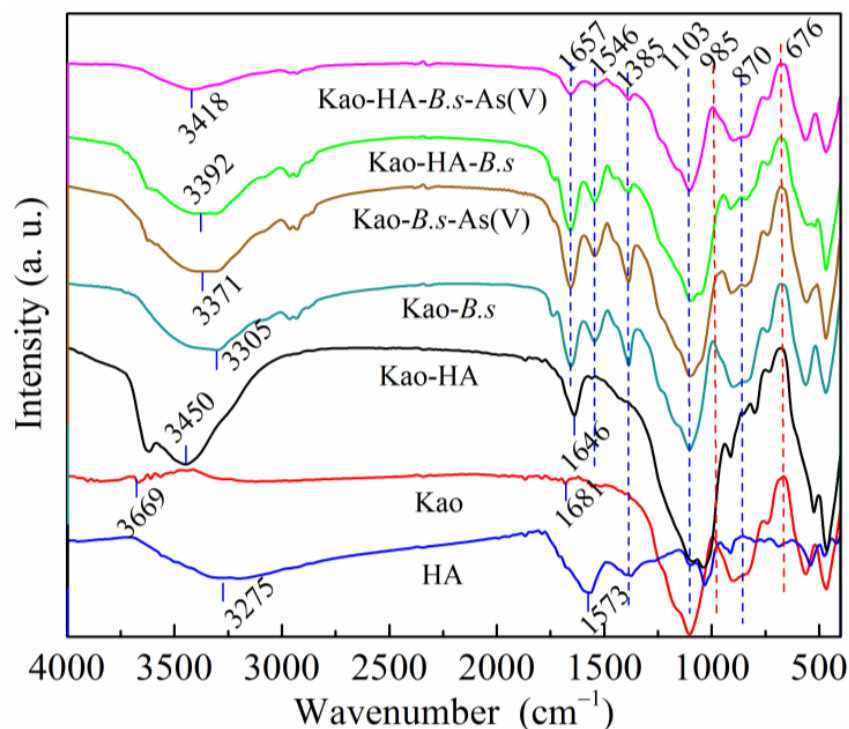


Figure 10. FT-IR spectra of composites before and after reaction with As(V).

When compared to the FT-IR spectrum of kaolinite and humic acid, new adsorption peaks appeared after the adsorption of As(V) on the mineral-organic composites. The characteristic of the O-H stretching vibration of water in the complexes and the hydroxyl groups of the physically adsorbed water molecules contributed to the absorption band of kaolinite at ca. 3669 and 1681 cm^{-1} before As(V) adsorption [57]; conversely, a bathochromic shift for the O-H band (3418–3305 cm^{-1}) was observed in all the spectra of the *Kao-B.subtilis* and *Kao-HA-B.subtilis* composites after As(V) adsorption, which was characteristically enhanced after the bacteria and As(V) were adsorbed on the surface of the kaolinite due to the presence of SiO^- and AlO^- , which provide relatively strong interactions through inner-spherical surface interactions [39]. However, the intensity of this peak decreased in the ternary system for the inhibitory effect of HA, which was due to the partial coverage of the inner-sphere binding sites of kaolinite, which was also reported by Du and Wu [24,50,52]. Similar trends were observed in the vibrational bands corresponding to the phenolics (1385 cm^{-1}) and aromatics (1573 cm^{-1}) of pure HA spectra and for the C=O and N-H/N-C of amide (1657 and 1546 cm^{-1}) for *B.subtilis*. When compared to the binary complex of Kao-HA, the new spectra of the *Kao-HA-B.subtilis* system displayed band shifts for the O-H band (from 3450 to 3392 cm^{-1}) and C=O (from 1646 to 1657 cm^{-1}), and presented the N-H/N-C of amide (1546 cm^{-1}), indicating that the chemical interactions increased during bacteria adhesion to the Kao-HA composite.

The adsorption peaks at around 3418 cm^{-1} and 3371 cm^{-1} were attributed to As-O vibration; the peak shift intensities of these As-O peaks from those reported in the studies were the result of lower kaolinite and HA content [50,57]. The relative intensities of the bands at ca. 985 cm^{-1} and 676 cm^{-1} increased significantly after arsenate adsorption, which could arise from the replacement of hydroxyl groups existing on the composites with As(V) by surface complexation.

3.7. Adsorption Mechanism

Kaolinite, humic acid, and *Bacillus subtilis*, as represented by the most ubiquitous and abundant components in the soil, play a crucial role in the immobilization and transformation of both metals and metalloids. Based on the above analysis, surface complexation, and

electrostatic interactions are the main mechanisms for As(V) adsorption in mineral-organic binary and ternary systems.

Our results showed that the adsorption of As(V) in the binary systems of the Kao-HA or Kao-*B.subtilis* composites were a synergistic process, which was greater than that in single systems. Two possible explanations are as follows: (1) As(V) was able to penetrate the bacteria in the outer layer banded with the carboxyl groups and form various inner-sphere complexes with kaolinite due to the variable charges in the latter's gibbsite basal planes. (2) The arsenic ions initially adsorbed on the bacterial and/or humic acid surfaces (at lower HA content) were bound to the lower potential of humic acid. As the reaction proceeded, they would gradually transfer to the higher potential energy mineral functional groups through chemical bonds or co-ordinate covalent bonds, thus forming an internal layer complex. In the ternary Kao-HA-bacteria system, a significant inhibitory effect on As(V) binding was observed at a higher HA content due to the shielding effect, while a promoting effect was shown at a lower concentration due to the dispersion effect of HA on the kaolinite particles. In the thermodynamic models, the adsorption of As(V) by all composites was a spontaneous entropy increase reaction, indicating that the inner-sphere complexes were formed during the adsorption process.

When taken together in combination with previous findings, our results demonstrate a universal synergistic effect with respect to humic acid (from 0.3% to 2.0%) and bacteria, playing a promoting role in the adsorption of As(V) on soil clay minerals.

4. Conclusions

This research demonstrates that the interaction of As(V) with kaolinite in the presence of natural organic matter and bacteria depends more upon the properties of the clay than on the presence of organic matter. The adsorption kinetics of As(V) onto the humic acid-kaolinite-*Bacillus subtilis* or kaolinite-humic acid composites could be described by the pseudo-second-order equation, and the maximum adsorption capacity for As(V) was 3.97 and 4.66 mg·g⁻¹ at an initial arsenic concentration of 21.15 mg·L⁻¹, respectively, and the adsorption processes were controlled by chemisorption. The dominant adsorption mechanism was surface complexation via the hydroxyl groups that exist on kaolinite with As(V). The adsorption isotherms of the process were better described by the Freundlich isotherm model, revealing the endothermic and favorable nature of the adsorption process. HA (at lower content) and bacteria promoted the adsorption of As(V), and the adsorption performance in the ternary system was higher than that of the mineral-bacteria binary system and the mineral-humic acid system with the multivariate function of electrostatic forces, chemical interactions, steric hindrance, and mineral aggregation, whereas the adsorption site masking effect occurred in the ternary system with a higher HA content. The maximum adsorption capacities followed the order of Kao-HA-*B.s* (50:1:50) > Kao-*B.s* > *B.s* > Kao-HA-*B.s* (100:5:1) > Kao-HA > Kao.

Author Contributions: Conceptualization, M.X. and S.L.; methodology, M.X. and S.L.; formal analysis and investigation, S.Z. and J.G.; data curation, M.X. and S.Z.; writing-original draft preparation, M.X. and J.G.; writing-review and editing, M.X. and S.L.; visualization, M.X. and S.L.; funding acquisition, M.X. All authors have read and agreed to the published version of the manuscript.

Funding: This research was funded by the opening fund of the Key Laboratory for the environmental factor control of agro product quality safety (18nynzahj-2), and the Natural Science Foundation of Liaoning Province (No. 2022-MS-404) for the financial support.

Data Availability Statement: Data will be made available on request.

Conflicts of Interest: The authors declare that they have no known competing financial interests or personal relationships that could have appeared to influence the work reported in this paper.

References

1. Buschmann, J.; Kappeler, A.; Lindauer, U.; Kistler, D.; Berg, M.; Sigg, L. Arsenite and arsenate binding to dissolved humic acid: Influence of pH, type of humic acid, and aluminum. *Environ. Sci. Technol.* **2006**, *40*, 6015–6020. [[CrossRef](#)]
2. Oliver, M.A. Soil and human health: A review. *Eur. J. Soil Sci.* **1997**, *48*, 573–592. [[CrossRef](#)]
3. Du, H.H.; Chen, W.L.; Cai, P.; Rong, X.X.; Dai, K.; Peacock, C.L.; Huang, Q.Y. Cd(II) sorption on montmorillonite-humic acid-bacteria composites. *Sci. Rep.* **2016**, *6*, 19499. [[CrossRef](#)]
4. Fakour, H.; Lin, T.F. Experimental determination and modeling of arsenic complexation with humic and fulvic acids. *J. Hazard. Mater.* **2014**, *279*, 569–578. [[CrossRef](#)]
5. Xu, S.Z.; Xing, Y.H.; Liu, S.; Luo, X.S.; Chen, W.L.; Huang, Q.Y. Co-effect of minerals and Cd(II) promoted the formation of bacterial biofilm and consequently enhanced the sorption of Cd(II). *Environ. Pollut.* **2020**, *258*, 113774. [[CrossRef](#)]
6. Manning, B.A.; Goldberg, S. Adsorption and stability of arsenic (III) at the clay mineral-water interface. *Environ. Sci. Technol.* **1997**, *31*, 2005–2011. [[CrossRef](#)]
7. Saada, A.; Breeze, D.; Crouzet, C.; Cornu, S.; Baranger, P. Adsorption of arsenic(V) on kaolinite and on kaolinite-humic acid complexes role of humic acid nitrogen groups. *Chemosphere* **2003**, *51*, 757–763. [[CrossRef](#)]
8. Root, R.A.; Dixit, S.; Campbell, K.M.; Jew, A.D.; Hering, J.G.; O'Day, P.A. Arsenic sequestration by sorption processes in high-iron sediments. *Geochim. Cosmochim. Acta* **2007**, *71*, 5782–5803. [[CrossRef](#)]
9. Saeedi, M.; Li, L.Y.; Grace, J.R. Desorption and mobility mechanisms of co-existing polycyclic aromatic hydrocarbons and heavy metals in clays and clay minerals. *J. Environ. Manag.* **2018**, *214*, 204–214. [[CrossRef](#)]
10. Giles, D.E.; Mohapatra, M.; Issa, T.B.; Anand, S.; Singh, P. Iron and aluminum based adsorption strategies for removing arsenic from water. *J. Environ. Manag.* **2011**, *92*, 3011–3022. [[CrossRef](#)]
11. Zhao, Y.J.; Xiao, M.; Zhao, S.; Fan, H. Enhanced adsorption of As(V) from aqueous solution by mesoporous goethite: Kinetics, isotherms, thermodynamics, and mechanism. *Desalination Water Treat.* **2020**, *201*, 250–260. [[CrossRef](#)]
12. Zhou, Y.; Yao, J.; He, M.Y.; Choi, M.M.F.; Feng, L.; Chen, H.L.; Wang, F.; Chen, K.; Zhuang, R.S.; Maskow, T.; et al. Reduction in toxicity of arsenic(III) to *Halobacillus* sp. Y35 by Kaolin and their related adsorption studies. *J. Hazard. Mater.* **2010**, *176*, 487–494. [[CrossRef](#)]
13. Matusik, J. Arsenate, orthophosphate, sulfate, and nitrate sorption equilibria and kinetics for halloysite and kaolinites with an induced positive charge. *Chem. Eng. J.* **2014**, *246*, 244–253. [[CrossRef](#)]
14. Redman, A.D.; Macalady, D.L.; Ahmann, D. Natural organic matter affects arsenic speciation and sorption onto hematite. *Environ. Sci. Technol.* **2002**, *36*, 2889–2896. [[CrossRef](#)]
15. Lin, H.T.; Wang, M.C.; Li, G.C. Complexation of arsenate with humic substance in water extract of compost. *Chemosphere* **2004**, *56*, 1105–1112. [[CrossRef](#)]
16. Roulia, M. Humic substances: A novel eco-friendly fertilizer. *Agronomy* **2022**, *12*, 754. [[CrossRef](#)]
17. Gustafsson, J.P. Arsenate adsorption to soils: Modelling the competition from humic substances. *Geoderma* **2006**, *136*, 320–330. [[CrossRef](#)]
18. Weng, L.P.; Riemsdiik WH, V.; Hiemstra, T. Effects of fulvic and humic acids on arsenate adsorption to goethite: Experiments and modeling. *Environ. Sci. Technol.* **2009**, *43*, 7198–7204. [[CrossRef](#)]
19. Li, Q.; Wang, Y.H.; Li, Y.C.; LLi, F.; Tang, M.D.; Hu, W.F.; Chen, L.; Ai, S.Y. Speciation of heavy metals in soils and their immobilization at micro-scale interfaces among diverse soil components. *Sci. Total Environ.* **2022**, *825*, 153862. [[CrossRef](#)]
20. Matusik, J.; Scholtzova, E.; Tunega, D. Influence of synthesis conditions on the formation of a kaolinite-methanol complex and simulation of its vibrational spectra. *Clays Clay Miner.* **2012**, *60*, 227–239. [[CrossRef](#)]
21. Gao, X.D.; Yang, G.; Tian, R.; Ding, W.Q.; Hu, F.N.; Liu, X.M.; Li, H. Formation of sandwich structure through ion adsorption at the mineral and humic interfaces: A combined experimental computational study. *J. Mol. Struct.* **2015**, *1093*, 96–100. [[CrossRef](#)]
22. Bauer, M.; Blodau, C. Mobilization of arsenic by dissolved organic matter from iron oxides, soils and sediment. *Sci. Total Environ.* **2006**, *354*, 179–190. [[CrossRef](#)]
23. Chen, C.; Dynes, J.J.; Wang, J.; Sparks, D.L. Properties of Fe-organic matter associations via coprecipitation versus adsorption. *Environ. Sci. Technol.* **2014**, *48*, 13751–13759. [[CrossRef](#)]
24. Du, H.H.; Nie, N.; Rao, W.K.; Lu, L.; Lei, M.; Tie, B.Q. Ferrihydrite-organo composites are a suitable analog for predicting Cd(II)-As(V) coexistence behaviors at the soil solid-liquid interfaces. *Environ. Pollut.* **2021**, *290*, 118040. [[CrossRef](#)]
25. Zou, Q.; Wei, H.; Chen, Z.L.; Ye, P.; Zhang, J.Q.; Sun, M.Q.; Huang, L.; Li, J. Soil particle size fractions affect arsenic (As) release and speciation: Insights into dissolved organic matter and functional genes. *J. Hazard. Mater.* **2023**, *443*, 130100. [[CrossRef](#)]
26. Xu, H.; Allard, B.; Grimvall, A. Influence of pH and organic substance on the adsorption of As(V) on geological materials. *Water Air Soil Pollut.* **1988**, *40*, 293–305. [[CrossRef](#)]
27. Cornu, S.; Saada, A.; Breeze, D.; Gauthier, S.; Baranger, P. Influence de composés organiques sur l'adsorption de l'arsenic par les kaolinites. *C. R. Acad. Sci.* **1999**, *328*, 649–654. [[CrossRef](#)]
28. Bauer, M.; Blodau, C. Arsenic distribution in the dissolved, colloidal and particulate size fraction of experimental solutions rich in dissolved organic matter and ferric iron. *Geochem. Cosmochim. Acta* **2009**, *73*, 529–542. [[CrossRef](#)]
29. Cui, J.; Jing, C. A review of arsenic interfacial geochemistry in groundwater and the role of organic matter. *Ecotoxicol. Environ. Saf.* **2019**, *183*, 109550. [[CrossRef](#)]

30. Aftabtalab, A.; Rinklebe, J.; Shaheen, S.M.; Niazi, N.K.; Moreno-Jimenez, E.; Schaller, J.; Knorr, K.H. Review on the interactions of arsenic, iron (oxy)(hydr)oxides, and dissolved organic matter in soils, sediments, and groundwater in a ternary system. *Chemosphere* **2022**, *286*, 131790. [[CrossRef](#)]
31. Fang, L.C.; Cai, P.; Li, P.X.; Wu, H.Y.; Liang, W.; Rong, X.M.; Chen, W.L.; Huang, Q.Y. Microcalorimetric and potentiometric titration studies on the adsorption of copper by *P. putida* and *B. thuringiensis* and their composites with minerals. *J. Hazard. Mater.* **2010**, *181*, 1031–1038. [[CrossRef](#)]
32. Hong, Z.N.; Chen, W.L.; Rong, X.M.; Cai, P.; Tan, W.F.; Huang, Q.Y. Effects of humic acid on adhesion of *Bacillus subtilis* to phyllosilicates. *Chem. Geol.* **2015**, *416*, 19–27. [[CrossRef](#)]
33. Rong, X.M.; Huang, Q.Y.; Chen, W.L. Microcalorimetric investigation on the metabolic activity of *Bacillus thuringiensis* as influenced by kaolinite, montmorillonite and goethite. *Appl. Clay Sci.* **2007**, *38*, 97–103. [[CrossRef](#)]
34. Wu, H.; Chen, W.; Rong, X.M.; Cai, P.; Dai, K.; Huang, Q.Y. Soil colloids and minerals modulate metabolic activity of *Pseudomonas putida* measured using microcalorimetry. *Geomicrobiol. J.* **2014**, *31*, 590–596. [[CrossRef](#)]
35. Li, S.F.; You, T.T.; Guo, Y.; Yao, S.H.; Zang, S.Y.; Xiao, M.; Zhang, Z.G.; Shen, Y.M. High dispersions of nano zero valent iron supported on biochar by one-step carbothermal synthesis and its application in chromate removal. *RSC Adv.* **2019**, *9*, 12428–12435. [[CrossRef](#)]
36. Wang, H.W.; Wang, Y.N.; Sun, Y.J.; Pan, X.L.; Zhang, D.Y.; Tsang, Y.F. Differences in Sb(V) and As(V) adsorption onto a poorly crystalline phyllosilicate (δ -MnO₂): Adsorption kinetics, isotherms, and mechanisms. *Process Saf. Environ. Prot.* **2018**, *113*, 40–47. [[CrossRef](#)]
37. Chen, R.Z.; Zhang, Z.Y.; Feng, C.P.; Lei, Z.F.; Li, Y.; Li, M.; Shimizu, K.; Sugiura, N. Batch study of arsenate (V) adsorption using Akadama mud: Effect of water mineralization. *Appl. Surf. Sci.* **2010**, *256*, 2961–2967. [[CrossRef](#)]
38. Yazdani, M.R.; Tuutijärvi, T.; Bhatnagar, A.; Vahala, R. Adsorptive removal of arsenic(V) from aqueous phase by feldspars: Kinetics, mechanism, and thermodynamic aspects of adsorption. *J. Mol. Liq.* **2016**, *214*, 149–156. [[CrossRef](#)]
39. Yusof, M.S.M.; Othman, M.H.D.; Wahab, R.A.; Jumbri, K.; Razak, F.I.A.; Kurniawan, T.A.; Samah, R.A.; Mustafa, A.; Rahman, M.A.; Jaafar, J.; et al. Arsenic adsorption mechanism on palm oil fuel ash (POFA) powder suspension. *J. Hazard. Mater.* **2020**, *383*, 121214. [[CrossRef](#)]
40. Walker, S.G.; Flemming, C.A.; Ferris, F.G.; Beveridge, T.J.; Bailey, G.W. Physicochemical interaction of *Escherichia coli* cell envelopes and *Bacillus subtilis* cell walls with two clays and ability of the composite to immobilize heavy metals from solution. *Appl. Microbiol. Biotechnol.* **1989**, *55*, 2976–2984. [[CrossRef](#)]
41. Qu, C.C.; Chen, W.L.; Hu, X.P.; Cai, P.; Chen, C.G.; Yu, X.Y.; Huang, Q.Y. Heavy metal behaviour at mineral-organic interfaces: Mechanisms, modelling and influence factors. *Environ. Int.* **2019**, *131*, 104995. [[CrossRef](#)]
42. Yan, Y.P.; Wan, B.; Mansor, M.; Wang, X.M.; Zhang, Q.; Kappler, A.; Feng, X.H. Co-sorption of metal ions and inorganic anions/organic ligands on environmental minerals: A review. *Sci. Total Environ.* **2022**, *803*, 149918. [[CrossRef](#)]
43. Ladeira, A.C.Q.; Ciminelli, V.S.T.; Duarte, H.A.; Alves, M.C.M.; Ramos, A.Y. Mechanism of anion retention from EXAFS and density functional calculations: Arsenic(V) adsorbed on gibbsite. *Geochim. Cosmochim. Acta.* **2001**, *65*, 1211–1217. [[CrossRef](#)]
44. Goldberg, S.; Johnston, C.T. Mechanisms of arsenic adsorption on amorphous oxides evaluated using macroscopic measurements, vibrational spectroscopy, and surface complexation modeling. *J. Colloid Interface Sci.* **2001**, *234*, 204–216. [[CrossRef](#)]
45. Naidu, R.; Bolan, N.S.; Kookana, R.S.; Tiller, K.G. Ionic-strength and pH effects on the sorption of cadmium and the surface charge of soils. *Eur. J. Soil Sci.* **1994**, *45*, 419–429. [[CrossRef](#)]
46. Ogata, F.; Ueta, E.; Kawasaki, N. Characteristics of a novel adsorbent Fe-Mg-type hydrotalcite and its adsorption capability of As(III) and Cr(VI) from aqueous solution. *J. Ind. Eng. Chem.* **2018**, *59*, 56–63. [[CrossRef](#)]
47. Deonarine, A.; Kolker, A.; Doughten, M.W.; Holland, J.T.; Bailoo, J.D. Mobilization of arsenic from coal fly ash in the presence of dissolved organic matter. *Appl. Geochem.* **2021**, *128*, 104950. [[CrossRef](#)]
48. Song, W.; Zhang, M.; Liang, J.; Han, G.M. Removal of As(V) from wastewater by chemically modified biomass. *J. Mol. Liq.* **2015**, *206*, 262–267. [[CrossRef](#)]
49. Ozer, A.; Akkaya, G.; Turabik, M. The biosorption of acid red 337 and acid blue 324 on *Enteromorpha prolifera*: The application of nonlinear regression analysis to dye biosorption. *Chem. Eng. J.* **2005**, *112*, 181–190. [[CrossRef](#)]
50. Xiao, Z.Y.; Xie, X.J.; Pi, K.F.; Gong, J.M.; Wang, Y.X. Effects of arsenic-iron-dissolved organic matter interactions on arsenic mobilization: Insight from column experiments. *J. Hydrol.* **2023**, *616*, 12837. [[CrossRef](#)]
51. Roulia, M.; Vassiliadis, A.A. Water purification by potassium humate-C. I. basic blue 3 adsorption-based interactions. *Agronomy* **2021**, *11*, 1625. [[CrossRef](#)]
52. Wu, P.X.; Zhang, Q.; Dai, Y.P.; Zhu, N.W.; Dang, Z.; Li, P.; Wu, J.H.; Wang, X.D. Adsorption of Cu(II), Cd(II) and Cr(III) ions from aqueous solutions on humic acid modified Ca-montmorillonite. *Geoderma* **2011**, *164*, 215–219. [[CrossRef](#)]
53. Chassapis, K.; Roulia, M.; Tsigirigi, D. Chemistry of metal-humic complexes contained in Megalopolis lignite and potential application in modern organomineral fertilization. *Int. J. Coal Geol.* **2009**, *78*, 288–295. [[CrossRef](#)]
54. Coppin, F.; Berger, G.; Bauer, A.; Caster, S.; Loubet, M. Sorption of lanthanides on smectite and kaolinite. *Chem. Geol.* **2002**, *182*, 57–68. [[CrossRef](#)]
55. Zhou, M.; Yang, R.J.; Tan, X.Y.; Yie, B.Q.; Lei, M.; Du, H.H. A universal synergistic rule of Cd(II)-Sb(V) coadsorption to typical soil mineral and organic components. *Adsorp. Sci. Technol.* **2022**, *2022*, 9131597. [[CrossRef](#)]

56. Liu, Y.L.; Walker, H.W.; Lenhart, J.J. The effect of natural organic matter on the adsorption of microcystin-LR onto clay minerals. *Colloids Surf. A Physicochem. Eng. Asp.* **2019**, *583*, 123964. [[CrossRef](#)]
57. Xie, X.J.; Liu, Y.Q.; Pi, K.F.; Liu, C.X.; Li, J.X.; Duan, M.Y.; Wang, Y.X. In situ Fe-sulfide coating for arsenic removal under reducing conditions. *J. Hydrol.* **2016**, *534*, 42–49. [[CrossRef](#)]

Disclaimer/Publisher’s Note: The statements, opinions and data contained in all publications are solely those of the individual author(s) and contributor(s) and not of MDPI and/or the editor(s). MDPI and/or the editor(s) disclaim responsibility for any injury to people or property resulting from any ideas, methods, instructions or products referred to in the content.